2013 IEEE/RSJ International Conference on
Intelligent Robots and Systems (IROS)
November 3-7, 2013. Tokyo, Japan

Standing Posture Modeling and Control for a Humanoid Robot

Syeda Mariam Ahmed, Chee Meng Chew, Bo Tian, *Member, IEEE*

***Abstract*— This paper presents a novel approach employing nonlinear control for stabilization of standing posture for a humanoid robot using only hip joint. The robot is modeled as an acrobot where model parameters are estimated through adaptive algorithm. A *'non-collocated partial feedback'* controller is applied. This is integrated with a *linear feedback* control, through LQR. Improved robustness to external push is demonstrated through evaluation in Webots simulator and on a physical humanoid robot, NUSBIP-III ASLAN. Performance comparison with other controllers verifies the effectiveness of the proposed control system.**

I. Introduction

When a human is pushed, the impulsive reaction is a synergy of control actions adopted by our upper and lower body. Multiple degrees of freedom provide the ability to sustain balance under constraints on individual joints, which may be imposed based on varying terrain and environment conditions.

For humanoid robots, push recovery has been investigated diversely in terms of varying control objectives. For compliant robots, balance is resolved through contact force control. This has been achieved by passivity based controllers where optimal contact force distribution leads to desired ground applied forces converted to joint torques [1-4]. Dynamic balance force control is another method which uses virtual model control to perform posture regulation for Sarcos Primus [5]. A similar method deals with defining desired rate of change of angular and linear momentum, based on computation of individual foot ground reaction forces (GRF) and center of pressure (CoP) [6]. [7-8] have attempted dynamic stabilization through optimization.

A slightly different approach is to reduce the humanoid to simple models and analyze their behavior in presence of disturbance. Linearized models constrained in a two-dimensional plane are controlled to yield desired ankle and hip trajectories which ensure center of mass (CoM) regulation above CoP [9-10]. These models have also been used by biomechanists to explain balancing through *ankle* and *hip* strategies for humans [11].

Modern *ankle* strategy for humanoid robots essentially abides by the ZMP theory and suggests employing ankle torque to regulate CoP within the convex hull formed by the support polygon. *Hip* strategy on the other hand, is used when ankle torque cannot alone sustain balance, and a restoring torque is applied at the hip in an attempt to restore CoM.

S. M. Ahmed and C. M. Chew are with the National University of Singapore, Singapore, {email: mariam.ahmed, chewcm }@nus.edu.sg.

Bo Tian is with Institute of Infocomm Research, A*STAR, Singapore, {email: btian@i2r.a-star.edu.sg}.

Fig. 1. Humanoid robot NUSBIP-III ASLAN used for experimentation in this paper

The approach adopted in this paper aims to use only hip joint to stabilize the system. This is to explore the effectiveness of hip joint to sustain balance using a passive ankle joint. Eliminating the compulsion of the ankle joint can lead to weight reduction by removing it from our humanoid robot NUSBIP III ASLAN. This in turn can facilitate swifter movement of the swing leg due to lighter inertia, especially as viewed from the hip joint.

Main contribution of this work is the use of nonlinear feedback for stabilization through the hip. Since the controller uses dynamics of the model for feedback, parameter estimation has to be carried out for our humanoid robot, through adaptive algorithm. The nonlinear controller is integrated with a linearized model for quicker posture regulation. The overall control system is tested in Webots simulator, followed by experimental evaluation on the physical robot.

The remainder of this paper is organized as follows. Section II discusses details regarding acrobot model and adaptive algorithm for parameter estimation. Section III describes the derivation of linear and nonlinear controllers. Section IV details the testing carried in the Webots simulator while section V evaluates hardware implementation results. Section VI discusses concluding remarks and directions for future work.

II. Model Based Parameter Identification for Humanoid Robots

Identification of inertial and frictional parameters for a humanoid robot is a highly complex task. Common identification approaches, generally used for robotic manipulators, like least square estimation, require design of identification trajectories that can excite the dynamics of the links. If under-actuation is present, it is challenging to design such trajectories.

For the robot ASLAN, initial estimates of total mass, link lengths, center of mass and inertia were derived from CAD of the biped. However friction, which plays a significant role in the dynamic equation, cannot be similarly estimated. This section introduces an adaptive control approach which estimates the parameters of the humanoid robot, based on a simplified model of a standing humanoid robot.

A. *Simplified Modeling*

The acrobot model in Fig 2, is chosen to represent the humanoid, which is equivalent to a double inverted pendulum with one passive and one active joint [12].

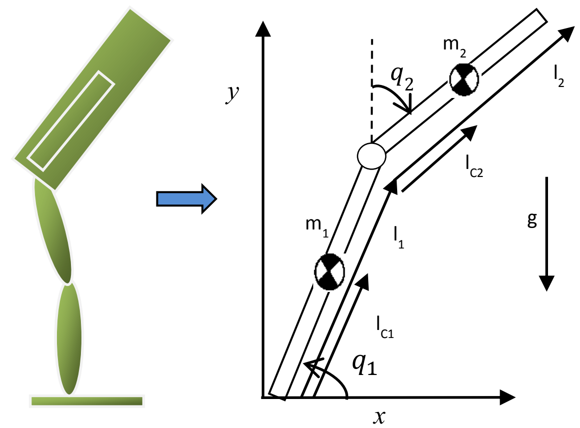

Fig. 2. Acrobot model for a standing humanoid robot

In this case, ankle joint is kept passive by turning off the current, while hip joint remains actuated. The equation of motion for the model is described as,

$$\tau = D(q)\ddot{q} + C(q,\dot{q})\dot{q} + F(\dot{q}) + G(q) \tag{1}$$

where q is the 2×1 vector of joint displacements, τ is the 2×1 vector of applied torques, $D(q)$ is the 2×2 positive definite inertia matrix. C is the 2×1 vector of centripetal and coriolis torques, $G(q)$ is the 2×1 vector of gravitational torques and F is the 2×1 vector of frictional torques induced by the gears and bearings in the robot. The friction model used is of the form [13],

$$F(\dot{q}) = f_c\frac{1-e^{-\dot{q}\alpha}}{1+e^{-\dot{q}\alpha}} + f_v\dot{q} \qquad \alpha = 10 \tag{2}$$

where f_c and f_v represent coulomb and viscous friction parameters, respectively. The use of the bipolar sigmoid term for the coulomb friction provides a continuous function, simplifying differentiation for linearization of nonlinear model for control design. This model also assumes that both legs move together at all times, therefore are modeled as a single link.

B. *Parameter Estimation through Adaptive Controller*

Adaptive controller [14] is used to estimate the parameters of the model described above. This method provides a strategy which is sensitive to unmodeled dynamics and attempts to keep track of the difference between the desired and actual trajectories while updating the parameters to minimize the resultant error.

The parameters for the adaptation algorithm are as follows,

$$\begin{aligned}
P_1 &= m_1 l_{c1}^2 + m_2 l_1^2 + I_1\\
P_2 &= m_2 l_{c2}^2 + I_2\\
P_3 &= m_2 l_1 l_{c2}\\
P_4 &= (m_1 l_{c1} + m_2 l_1)g\\
P_5 &= m_2 l_{c2} g\\
P_6 &= f_{cAnkle}\\
P_7 &= f_{vAnkle}\\
P_8 &= f_{cHip}\\
P_9 &= f_{vHip}
\end{aligned} \tag{3}$$

For parameter estimation, the ankle and hip joints have been made to follow simple sinusoidal trajectories with varying amplitudes and frequencies. The final values obtained at the end of this experiment have been tabulated in Table 1.

Table1. Final parameters values

PARAMETER	ESTIMATED	PARAMETER	ESTIMATED
$\hat{P}_1$	5.309	$\hat{P}_6$	0.200
$\hat{P}_2$	0.8020	$\hat{P}_7$	-2.780
$\hat{P}_3$	1.510	$\hat{P}_8$	0.500
$\hat{P}_4$	88.18	$\hat{P}_9$	-23.50
$\hat{P}_5$	26.45		

III. PUSH RECOVERY ALGORITHM

When encountering a forward or backward push, the robot rotates about its ankle. In order to stabilize the system using the actuated degree of freedom at the hip, design of a nonlinear control strategy for the derived model is explored. The controller strategy described aims to linearize the passive degree of freedom through nonlinear controller, to move the disturbed system to the desired equilibrium state.

A. *Passive Ankle Control using Non-Collocated Partial Feedback Linearization*

Partial feedback linearization approach estimates the desired torque based on nullification of nonlinearities proposed by Spong[15]. This approach has been implemented in two ways, namely *Collocated* and *Non-Collocated* linearization. This section introduces *Non-Collocated Partial Feedback Linearization* (NCPFL) control for control of the passive ankle through the hip joint.

The equation of motion derived from Eq 1, with an assumption of no ankle torque leads to,

$$d_{11}\ddot{q}_1 + d_{12}\ddot{q}_2 + G_1 + C_1 + F_1 = 0 \tag{4}$$

$$d_{21}\ddot{q}_1 + d_{22}\ddot{q}_2 + G_2 + C_2 + F_2 = \tau_{hip} \tag{5}$$

Eq. 4 can be rearranged as follows,

$$\ddot{q}_2 = -d_{12}{}^{-1}(\, d_{11}\ddot{q}_1 + G_1 + C_1 + F_1) \tag{6}$$

Substituting Eq. 6 in Eq. 5 yields the following expression,

$$\widetilde{M}_{21}\ddot{q}_1 + \tilde{C}_2 + \tilde{G}_2 + \tilde{F}_2 = \tau \tag{7}$$

Such that,

$$\widetilde{M}_{21} = d_{21} - d_{22}{d_{12}}^{-1}d_{11} \tag{8}$$

$$\tilde{C}_2 = C_2 - d_{22}{d_{12}}^{-1}C_1 \tag{9}$$

$$\tilde{G}_{21} = G_2 - d_{22}{d_{12}}^{-1}G_1 \tag{10}$$

$$\tilde{F}_2 = F_2 - d_{22}{d_{12}}^{-1}F_1 \tag{11}$$

The output controlled is the ankle joint displacement,

$$y = q_1 \tag{12}$$

Since the objective is to restore q_1 to its equilibrium state of $q_1^* = 90^o$, which represents a vertical configuration for the lower body, the following additional control input is added,

$$v_1 = \ddot{q}_1 \tag{13}$$

which is replaced by local PD control terms as follows,

$$v_1 = -K_{vD}\dot{q}_1 + K_{vP}\,(1.57 - q_1) \tag{14}$$

This input effectively reduces the dynamics of the lower link to a second order linear system. Local stability properties of this controller are explained in [15].

Even though this approach is effective for ankle joint stabilization, it leads to a few oscillations before reaching the desired posture. Thus the next section explores linear state feedback, in order to achieve faster convergence.

B. Posture Regulation through LQR

Having stabilized the ankle joint, the hip joint is required to maintain its position at $\boldsymbol{q_{2D}}^* = 0$. Since the system is in the vicinity of the desired state, a linear feedback controller is designed which ensures complete stabilization of the robot. For this purpose, the nonlinear equations of the system are linearized around q_{1D}^*, q_{2D}^*, where the state x is defined as,

$$x = [q_1, q_2, \dot{q}_1, \dot{q}_2]^T, \tag{15}$$

$$\boldsymbol{q} = [q_1, q_2]^T, \qquad \dot{\boldsymbol{q}} = [\dot{q}_1, \dot{q}_2]^T, \tag{16}$$

where q_1 and q_2 represent angular rotations for ankle and hip respectively, while $\dot{q}_1$ and $\dot{q}_2$ represent respective angular velocities. Employing Taylor series expansion, the nonlinear equations of motion result in a state space model, which is used to implement linear feedback on the system, as follows,

$$\dot{x} = \begin{bmatrix} 0_{2x2} & I_{2x2} \\ -D^{-1}\frac{\partial G}{\partial q} & -D^{-1}\frac{\partial F}{\partial \dot{q}} \end{bmatrix} \begin{bmatrix} q_1 \\ q_2 \\ \dot{q}_1 \\ \dot{q}_2 \end{bmatrix} + \begin{bmatrix} 0 \\ D^{-1}B \end{bmatrix} \begin{bmatrix} \tau_A \\ \tau_H \end{bmatrix} \tag{17}$$

In order to determine the optimal trajectory, after the push, towards the vertical position, an optimal feedback controller needs to be designed. Optimality has been defined in terms of a quadratic cost function as follows [12],

$$J = \tfrac{1}{2}\int \int_0^{\infty}(x^TQx + u^TRu)dt \tag{18}$$

$$Q = Q^T > 0, R = R^T > 0 \tag{19}$$

The linear feedback matrix u is defined as,

$$u = -Lx \tag{20}$$

where the L matrix is responsible for optimality in the linear quadratic regulator.

C. Full Body Control Architecture

A control architecture shown in Fig. 3 has been designed to implement push recovery in real time. At every sampling time, the state x, including angular rotations and velocities for ankle and hip, is estimated through motor encoders and IMU readings.

Locations of CoM_A and CoM_H (horizontal projections of ankle and hip joint angular displacements) of the chosen model determine which controller should be given priority over the other. Based on the boundary conditions defined below, a variable γ is introduced such that the value of γ is determined by,

$$\gamma = 0 \;\{\, CoM_A > 0.01 \;||\; CoM_A < -0.01 \tag{21}$$

$$\gamma = 1 \begin{cases} -0.01 < CoM_A < 0.01 \\ CoM_H > 0.005 \;||\; CoM_H < -0.005 \end{cases} \tag{22}$$

The final torque value commanded to the motor is given by the following,

$$\tau_H{}^* = \tau_{PFL}(1-\gamma) \;+\; \tau_{LQR}\gamma \tag{23}$$

This linear feedback is only used as a faster means of convergence when the hip joint is close to the desired state.The control strategy formulated defines torque for the hip joint. This is accompanied with a simple PD controller at the ankle,

$$\tau_A = K_{PA}\,(1.57 - q_1) - K_{DA}\dot{q}_1 \tag{24}$$

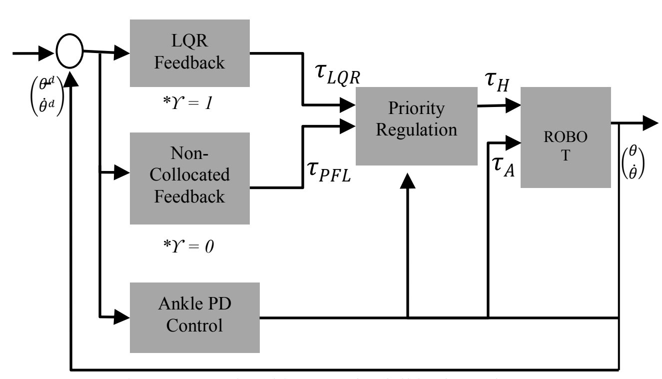

Fig. 3. Control architecture for full body push recovery

This torque is primarily to cater to the friction at the ankle joint, which acts highly rigid when ankle torque is zero, which will be verified in section V.

IV. SIMULATION RESULTS

A. Simulation Setup

Detailed testing of the proposed strategy has been carried out on the Webots robot simulator [16].The model of a humanoid robot shown in Fig 4, which has been designed in this environment with a total length of 1.7m and weight of 86.6Kg. Each limb of the humanoid consists of six degrees of freedom. The robot consists of 3-axis global positioning sensor (GPS) and 3-axis accelerometer, at the torso, for position and orientation sensing. The simulation and controller output is updated at a frequency of 125Hz.

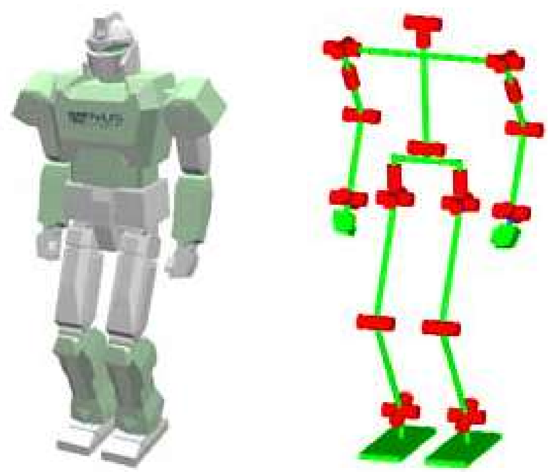

Fig. 4. Humanoid simulation model in webots

The robot is pushed using a "*ball*" robot model which has a mobile base. The ball is equipped with a force sensor which measures the impulse at impact with the humanoid. The height of the ball is at 1.2m such that the humanoid robot is pushed on the torso.

B. Implementation Details

The servos of the robot are operated in torque control mode, where the commanded torque is determined by Eq 28. The LQR controller is tuned in MATLAB where the values for Q and R matrices for state space model are given as Q = I(4x4) and R = 10e-12. The optimized L matrix is L = *[30.15, 147.4, -25.28 -27.48]*. No PD controller is required in simulation since the joints can be switched to torque mode where the ankle joint indeed remains passive.

With the parameters defined above, the simulation is tested under different impulse magnitude imparted to the humanoid from both front and back, restricted to sagittal plane only. An extra GPS is added at the location defined by CoM_{AVG} which is given as

$$CoM_{AVG} = \frac{m_1 * CoM_A + m_2 * CoM_H}{m_1 + m_2} \tag{25}$$

This enables determination of CoM_{AVG} linear position and velocity, which is employed for evaluation through phase plots.

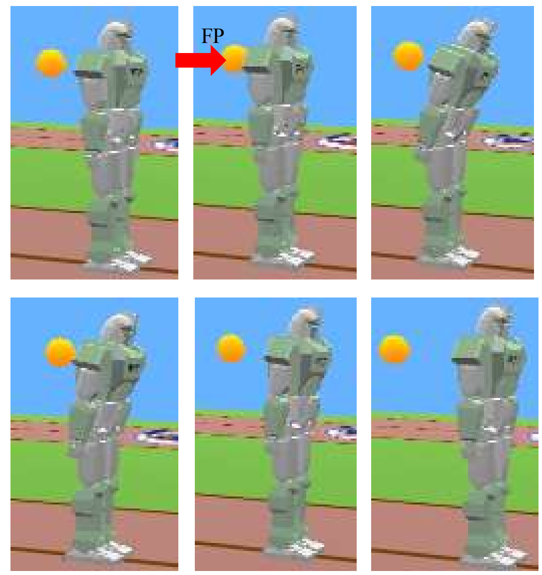

Fig. 5. Simulation response for forward push of 164Ns

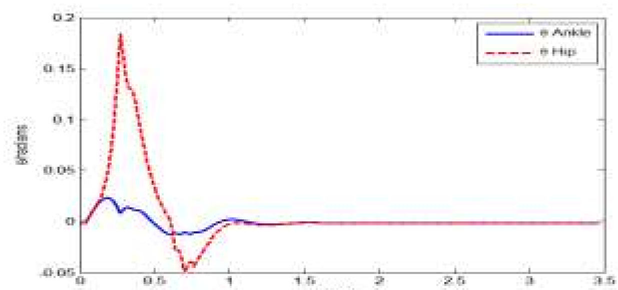

a) Angular Deflection

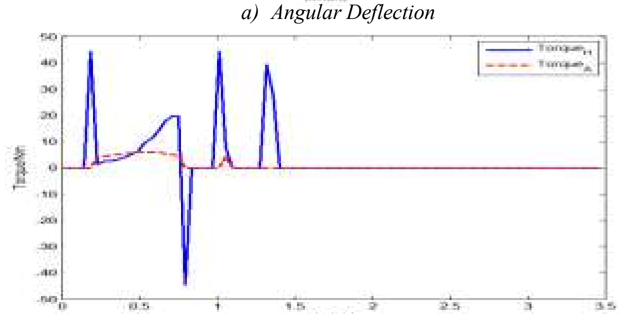

b) Applied Torque

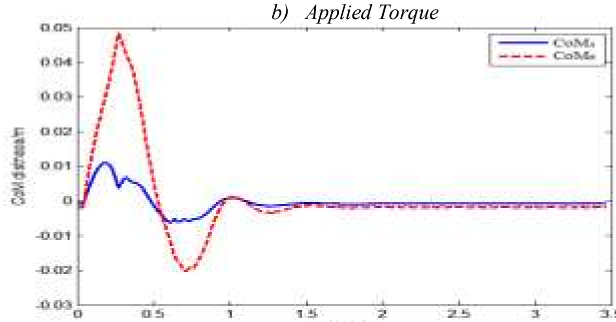

c) CoM_A and CoM_H Deflection

Fig. 6. Simulation response for push of 164Ns

C. Result Evaluation

Fig. 5 shows the response of the humanoid robot under an instantaneous disturbance of 164Ns from the back. The graphs shown in Fig. 6 reflect the ability of the controller to cater disturbances of such large magnitude. The graph also shows minimum dependence of less than 10Nm on ankle torque while the saturation limits go much beyond this value.

The phase plot in figure 7 shows the stability margin for CoM_{AVG} of the simulated robot. The stable and unstable regions have been achieved by experimentation on the simulator, for multiple trajectories with varying magnitudes of force applied. The shaded area in this figure corresponds to the unstable region. In this region, disturbances causing an instantaneous CoM_{AVG} velocity shift beyond 0.45ms^{-1} lead to an unstable trajectory. Such levels of disturbance should be catered by taking a step.

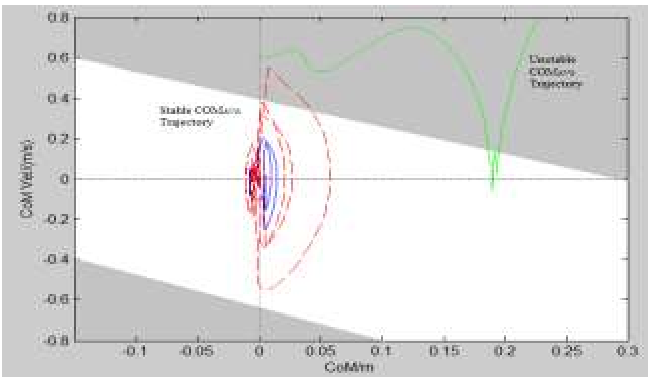

Fig. 7. Phase plot for multiple trajectories for CoM_{AVG}

V. EXPERIMENTATION RESULTS

A. Hardware Platform

The robot NUSBIP-III ASLAN at NUS is used for implementation of the controller designed above. ASLAN is a human sized humanoid robot equipped with DC servo motors which are controlled through ELMO amplifiers. PC/104 is the major processing unit with a processing frequency of 100Hz, which communicates with ELMO through CAN BUS.

The robot is equipped with accelerometers and rate gyroscopes to provide inertial measurement. Rotational joint measurements are sensed through encoders mounted at the motors.

B. Implementation Details

The servos of the robot are operated in current mode, where the commanded current is determined as follows,

$$i = \frac{\tau}{K_T N} \tag{26}$$

where K_T and N represent torque constant specified in the motor datasheet, and gear ratio respectively. Since the weight and size of the simulated and actual robots are different, the new L matrix is defined as $L = [10.15, 165.7, -15.28\ -7.25]$. The gains employed at the ankle for PD control are $K_{DA} = 0.5$, and $K_{PA} = 55$.

C. Result Evaluation

Figure 8 shows graphs for multiple push imparted to the humanoid from front and back. It can be seen from Figure 8b that the maximum ankle current employed is $-1.5<i_A<1.5$ amperes, where the ankle motor has the capacity to provide up to 7 amperes of continuous current. Thus it is hypothesized that the current employed through PD controller assists to overcome ankle friction components during upper body movements determined by NCPFL. Figures 8a and c reflect the ability of the proposed strategy to cater disturbances applied to the robot in a sagittal plane. Figure 9 shows snapshots of the robot ASLAN responding to a push applied from front and back.

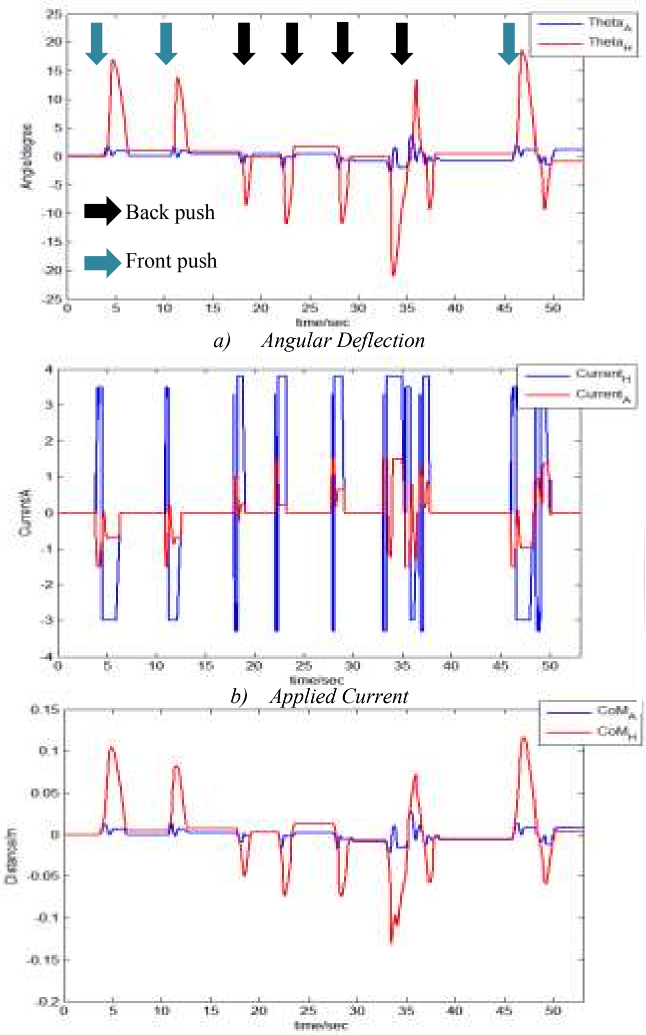

a) Angular Deflection

b) Applied Current

c) CoM_A and CoM_H Deflection

Fig. 8. ASLAN experimentation response to successive push

D. Performance Comparison with Passive Ankles

The proposed control architecture has been designed for an acrobot model which implies passive ankles for the robot. In the previous section, a PD controller was proposed to cater friction components at the ankle joint. This section completely removes any torque provided to the ankle and evaluates performance of various controllers under such "*zero ankle torque*" conditions. There are two objectives behind this experimentation. First, a comparison is conducted between NCPFL and other algorithms to compare the efficiency of the proposed algorithm. Second, it is proved that the torque provided to the ankle in the complete control strategy is indeed used only for friction compensation.

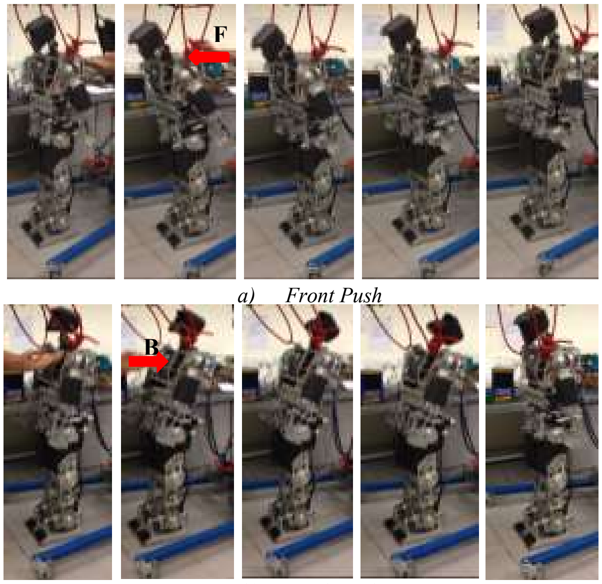

a) Front Push

b) Back Push

Fig. 9. Push recovery experimentation on ASLAN

NCPFL is implemented on the humanoid robot, compared with LQR and *Bang-Bang* [9] control approach. *Bang-Bang* controller is chosen since it is a common controller opted for the implementation of the *'hip strategy'*. The results obtained from this experimentation have been shown in Fig 10. The graphs show that *Bang-Bang* (BB) leads to oscillation before stabilization. This is because BB defines a fixed maximum and minimum current value for ankle restoration. LQR is able to restore the ankle, to a certain extent, but the convergence range over CoM_A is very limited. For higher ankle deflection, it commands current which is out of bounds for the actuators. Thus NCPFL proves to be a better option for the control of passive ankle through the hip joint.

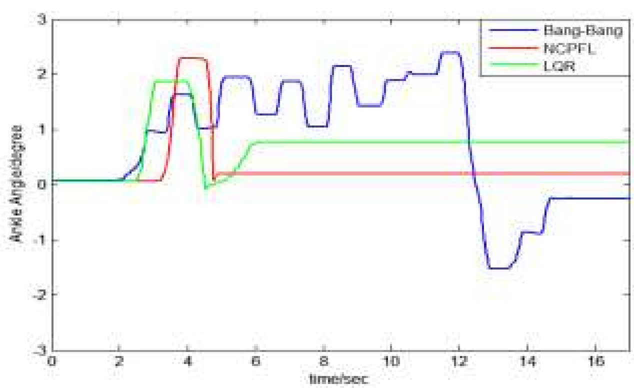

Figure 10. Performance Comparison for Passive Ankle Joint

Despite having the ability of restoration, it is observed during experimentation that a standalone NCPFL strategy with zero ankle torque employs large rotation of the upper body. Whereas, a small amount of regulating current at the ankles can significantly decrease this upper body bend. The hypothesized reason is associated with compensation of friction at the non-back drivable ankle joint which requires a larger jolt from the upper body under high friction. Thus the complete architecture for push recovery includes an ankle torque controller, to facilitate control attempted through the hip joint.

VI. Conclusion

In this paper, a synergy of NCPFL and LQR control is presented as an efficient mean to regulate the standing posture of the humanoid robot, when pushed. The proposed strategy has been tested in Webots and experimentally verified on NUSBIP-III ASLAN. A comparative analysis of the controller is provided, with other common control strategies. This analysis provides beneficial insights into practical considerations that need to be accounted for, in a position controlled humanoid, with essentially stiff joints.

Possible future work can include extension of this algorithm to take into consideration the knee joint as part of the stabilization process, since knee plays an important role in human stabilization techniques. The two link model can be extended to three links and may be compared with the work presented in this paper.

References

[1] S. Hyon and G. Cheng, "Passivity-based full-body force control for humanoids and application to dynamic balancing and locomotion," in *Proc. Of IEEE/RSJ International Conference on Intelligent Robots and Systems*, Beijing, China, Oct. 2006, pp. 4915-4922.

[2] S. H. Hyon, J. G. Hale and G. Cheng, "Full-body compliant human humanoid interaction: Balancing in the presence of unknown external forces," *IEEE Transactions on Robotics*, vol 23, pp. 884-898, October 2007.

[3] A. Albu-Schaffer, C. Ott, and G. Hirzinger, "A unified passivity-based control framework for position, torque and impedance control of flexible joint robots," *International Journal of Robotics Research*, vol. 26, no. 1, pp. 23-29, January 2007.

[4] C. Ott, A. Albu-Schaffer, A. Kugi, and G. Hirzinger, "On the passivity based impedance control of flexible joint robots," *IEEE Transactions Robotics*, vol. 24, no. 2, pp. 416-429, 2008.

[5] B. J. Stephens and C. G. Atkeson, "Dynamic balance force control for compliant humanoid robots," in *Proc. of International Conference on Intelligent Robots and Systems*, 2010.

[6] S. –h. Lee and A. Goswami, "Ground reaction force control at each foot: A momentum-based humanoid balance controller for non-level and non-stationary ground," in *IEEE/RSJ International Conference on Intelligent Robots and Automation*, May 2009, pp. 4423-4429.

[7] C. Atkeson and B. Stephens, "Multiple balance strategies from one optimization criterion," in *The IEEE-RAS 2007 International Conference on Humanoid Robots*, 2007.

[8] J. Wang, "Humanoid push recovery with robust convex synthesis," in *IEEE/RSJ International Conference on Intelligent Robots and Systems*, Oct. 2012.

[9] B. Stepehns, "Humanoid push recovery", *IEEE-RAS International Conference on Humanoid Robotics*, Pittsburgh, 2007.

[10] S.-J. Yi, B.-T. Zhang, D. Hong and D.D. Lee, "Learning full body push recovery control for small humanoid robots", *Proceedings of IEEE International Conference on Robotics and Automation*, 2011.

[11] D. Winter, "Human balance and posture control during standing and walking," *Gait and Posture*, vol. 3, no. 4, pp. 193-214, December 1995.

[12] Russ Tedrake, "Underactuated robotics: Learning, planning and control for efficient and agile machines", Course notes for MIT 6.832, *Masachusetts Institute of Technology,* 2009.

[13] M. Grotjahn, M. Daemi, and B. Heimann. "Friction and rigid body identification of robot dynamics". *International Journal of Solids Structure*, vol. 38, pp. 10-13, 2001.

[14] J.-J. Slotine and W. Li, "On the adaptive control of robot manipulators". *International Journal of Robotics Research*, pp. 49-59, 1987.

[15] M.W. Spong, "Partial feedback linearization of underactuated mechanical systems", *Proceedings of IEEE International Conference on Intelligent Robots and Systems*, pp. 314-321, 1994.

[16] Webots, http://www.cyberbotics.com, commercial Mobile Robot Simulation Software. [Online]. Available:http://www.cyberbotics.com